JOC Articles

Structural NMR and ab Initio Study of Salicylhydroxamic and *p*-Hydroxybenzohydroxamic Acids: Evidence for an Extended Aggregation

Begoña García,*[,§] Fernando Secco,*[,†] Saturnino Ibeas,[§] Asunción Muñoz,[§] Francisco. J. Hoyuelos,[§] José M. Leal,[§] María L. Senent,[‡] and Marcella Venturini[†]

Universidad de Burgos, Departamento de Química, 09001 Burgos, Spain, Universitá di Pisa, Dipartimento di Chimica e Chimica Industriale, 56126 Pisa, Italy, and Consejo Superior de investigaciones Cientificas, Departamento de Astrofisica Molecular e Infrarroja, Instituto de Estructura de la Materia, 28006 Madrid, Spain

begar@ubu.es; ferdi@dcci.unipi.it

Received May 9, 2007

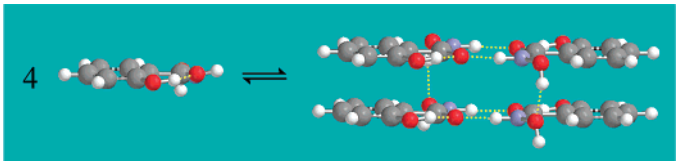

The acid−base behavior and self-aggregation of salicylhydroxamic (SHA) and *p*-hydroxybenzohydroxamic acids (PHBHA)have been investigated by UV and ^{1}HNMR spectroscopy, respectively. The acid−base parameters, measured in H_2O at 25 °C and $I = 0.1$ M, were $pK_1 = 7.56$, $pK_2 = 9.85$ for SHA and $pK_1 = 8.4$, $pK_2 = 9.4$ for PHBHA. The ^{1}H NMR signals for salicylhydroxamic and *p*-hydroxybenzohydroxamic acids measured in acetone indicate that both acids self-aggregate according to a mechanism where two monomers produce planar *E*−*E* dimers stabilized by horizontal H-bonds. Further dimer aggregation yields sandwich-like tetramer structures stabilized by vertical H-bonds and $\pi-\pi$ interactions. The *p*-hydroxybenzohydroxamic tetramers, less stable than those of salicylhydroxamic, contain two water molecules in their structures. The gas-phase structures of salicylhydroxamic acid and its anions were investigated by ab initio calculations using the density functional theory at the B3LYP/AUG-cc-pVDZ level. The SHA most stable gas-phase conformer is the A-*Z* amide, a structure with all three phenolate (O_P), carboxylate (O_C), and hydroxamate (O_H) oxygen atoms in the *cis* position. The B-*Z* amide, with the O_P oxygen *trans* to O_C, lies 5.4 kcal above the A-*Z* amide. The most stable monoanion is the N-deprotonated A-*Z* amide.

Introduction

Hydroxamic acids (R-CONHOH) are very important bioligands.[1] Much of their biological activity is related to their ability to form very stable metal chelates,[2] especially with iron.[3] The literature related with hydroxamic acids is very extended, as inferred from the growing amount of work published in the past few years, compiled in earlier publications.[4−6] Despite the renewed effort made to elucidate the main features and due to their ability to adopt different conformations, the solution chemistry of hydroxamic acids is still poorly characterized.[5] The restrained rotation around the C−N bond revealed by NMR

[§] Universidad de Burgos.
[†] Universitá di Pisa.
[‡] Instituto de Estructura de la Materia.

(1) Munson, J. W. In *Chemical Biology of Hydroxamic Acids*; Kehl, H., Ed.; Karger: New York, 1982; Chapter 1.
(2) Bauer, L.; Exner, O. *Angew. Chem., Int. Ed.* **1974**, *13*, 376−384.
(3) Raymond, K. N. *Coord. Chem. Rev.* **1990**, *105*, 135−153.
(4) Garcia, B.; Ibeas, S.; Leal, J. M.; Secco, F.; Venturini, M.; Senent, M. L.; Niño, A.; Muñoz, C. *Inorg. Chem.* **2005**, *44*, 2908−2919.
(5) García, B.; Ibeas, S.; Muñoz, A.; Leal, J. M.; Ghinami, C.; Secco, F.; Venturini, M. *Inorg. Chem.* **2003**, *42*, 5434−5441.
(6) Senent, M. L.; Niño, A.; Muñoz-Caro, A.; Ibeas, S.; García, B.; Leal, J. M.; Secco, F.; Venturini, M. *J. Org. Chem.* **2003**, *68*, 6535−6542.

10.1021/jo0709798 CCC: $37.00
Published on Web 09/21/2007

measurements,[7,8] and borne out by theoretical calculations,[4] gives rise to the *Z* and *E* conformers whose existence would imply the possible formation of the corresponding imide structures. However, ab initio and NMR investigations[4,6−8] suggest that formation of imide structures both in the undissociated hydroxamic acids and in their anions is in the minority. On the basis of theoretical calculations and comparative data with amides, some authors have concluded that the *Z*-amide conformation of the monohydroxamate group (CONHOH) becomes preferentially stabilized either by intramolecular hydrogen bonding in nonpolar solvents[9] or by hydrogen bonding with water molecules.[10] On the other hand, the *Z*-imide structure is definitely present in the hydroxamic acid/metal chelates.[4,5,11]

A further matter of debate stems from the acid−base properties of monohydroxamic acids. Apparently both the N−H and O−H protons are labile; however, different titration experiments with strong bases have shown that only one proton can be removed, even at the highest basicity levels. Therefore, the challenge of assigning the deprotonation site in monohydroxamic acids still remains. The O vs N deprotonation controversy has given way to different interpretations by different authors.[9,12] Thus far, the NMR experiments carried out indicate that both the N- and O-deprotonation progress to similar extents.[4−6] On the other hand, a number of gas-phase conformations supporting N-acidity[4,6,13,14] for the anions of formohydroxamic,[15] acetohydroxamic (AHA),[6,15−17] and benzohydroxamic acids (BHA) have been deduced from ab initio calculations.[4]

We report here on a theoretical and experimental investigation on salicylhydroxamic acid (SHA) and an experimental investigation on its isomer *p*-hydroxybenzohydroxamic acid (PHBHA); although these acids bear three potentially acidic hydrogen atoms, upon titration with bases only the phenol proton and one of the two remaining protons are prone to afford the corresponding anions.[18] Hence, this work is aimed at: (a) determining the most stable structure for both the undissociated species and its anions, identifying the most likely SHA gas-phase ionization sites; (b) evaluating by UV−vis spectrophotometry the SHA and PHBHA pK_A deprotonation values in water, and deriving conclusions on their acidic behavior; and (c) extracting information about the PHBHA and SHA structures from ^{1}H NMR spectra in deuterated acetone.

TABLE 1. Calculated Relative Energy (kcal/mol) and Dipole Moment (Debyes) of the Neutral Forms and Anions, and Dissociation Energies (kcal/mol) of A-SHA with the B3LYP/AUG-cc-pVDZ

neutral forms	E_R	μ
A-*Z*-amide	0.0[a]	3.1288
A-*E*-amide	4.5	3.7061
anions	E_R	μ
A-*Z*-1	0.0[b]	5.5199
A-*Z*-2	13.8	8.9918
A-*Z*-3	15.4	4.6997
A-*E*-1	12.7	4.6109
A-*E*-2	9.3	4.3444
A-*E*-3	22.2	4.1736
		dissociation energies
A-*Z*-amide ⇄ A-*Z*-1		335.7
A-*Z*-amide ⇄ A-*Z*-2		349.5
A-*Z*-amide ⇄ A-*Z*-3		351.2
A-*E*-amide ⇄ A-*E*-1		343.0
A-*E*-amide ⇄ A-*E*-2		340.5
A-*E*-amide ⇄ A-*E*-3		353.0

[a] E_a= −551.431548 au. [b] E_b= −550.896510 au.

Results and Discussion

Theoretical Study of SHA. To properly cope with the geometry optimization of both the neutral SHA species and its anions, the amide and imide *Z* and *E* forms with the aromatic ring coplanar with the O═C−N group were taken as starting structures. From here onward, O_C stands for the carbonyl oxygen, O_p for the phenolate oxygen, and O_H for the hydroxamate oxygen. The search for some stable forms has provided a set of 36 different SHA geometries (14 amide and 22 imide forms) among which the A and B conformation sets stand out. In the A-form, the ortho toluenic O_PH group faces the CO group, whereas in the B form the O_PH faces the nitrogen atom. Scheme 1 displays the most stable neutral and anionic A-SHA amide forms; Table 1 lists their relative energies and dipole moments calculated with the B3LYP/AUG-cc-pVDZ method. The remaining structures are stored in Scheme S1, and their parameters are set down in Table S1 of the Supporting Information (SI).

(7) Brown, D. A.; Glass, W. K.; Mageswaran, R.; Girmany, B. *Magn. Reson. Chem.* **1988**, *26*, 970−973.
(8) (a) Brown, D. A.; Glass, W. K.; Mageswaran, R.; Mohammed, S. A. *Magn. Reson. Chem.* **1991**, *29*, 40−45. (b) Brown, D. A.; Cufle, L. P.; Fitzpatrick, G. M.; Fitzpatrick, N. J.; Glass, W. K.; Herlihy, K. M. *Collect. Czech. Chem. Commun.* **2001**, *66*, 99−108.
(9) Lipczynska-Kochany, E.; Iwamura, H. *J. Org. Chem.* **1982**, *47*, 5277−5282.
(10) Brown, D. A.; Coogan, R. A.; Fitzpatrick, N. J.; Glass, W. K.; Abukshima, D. A.; Shiels, L.; Ahlgrén, M.; Smolander, K.; Pakkanen, T. T.; Peräkylä, M. *J. Chem. Soc., Perkin Trans. II* **1996**, 2673−2679.
(11) Dominey, L. A; Kustin, K. *Inorg. Chem.* **1984**, *23*, 103−108.
(12) (a) Exner, O.; Kakác, B. *Collect. Czech. Chem. Commun*. **1963**, *28*, 1656−1663. (b) Exner, O.; Holubek, J. *Collect. Czech. Chem. Commun* **1965**, *30*, 940−951. (c) Monzyk, B.; Crumbliss, A. L. *J. Org. Chem*. **1980**, *45*, 4670−4675. (d) Bordwell, F. G.; Fried, H. E.; Hughes, D. L.; Lynch, T. S.; Satish, A. V.; Whang, Y. E. *J. Org. Chem*. **1990**, *55*, 3330−3336. (e) Bagno, A.; Comuzzi, C.; Scorrano, G. *J. Am. Chem. Soc*. **1994**, *116*, 916−924. (f) Bordwell, F. G.; Liu, W. Z. *J. Am. Chem. Soc*. **1996**, *118*, 10819−10823. (g) Bagno, A.; Scorrano, G. *J. Phys. Chem*. **1996**, *100*, 1536−1544. (h) Bagno, A.; Dorigo, F.; McCrae, P.; Scorrano, G. *J. Chem. Soc. Perkin Trans. II* **1996**, 2163−2168.
(13) (a) Pranata, J. *J. Comput. Chem.* **1993**, *14*, 685−690. (b) Niño, A.; Muñoz-Caro, C.; Senent, M. L. *J. Mol. Struct.* (*THEOCHEM*) **2000**, *530*, 291−300.
(14) (a) Hupe, D. J.; Wu, D. *J. Am. Chem. Soc*. **1977**, *99*, 7653−7659. (b) Yamaki, R. T.; Paniago, E. B.; Carvalho, S.; Howarth, O. W.; Kam, W. *J. Chem. Soc., Dalton Trans*. **1997**, *24*, 4817−4821. (c) Keeffe, J. R.; Jencks, W. P. *J. Am. Chem. Soc*. **1983**, *105*, 265−279. (d) Liu, S. X.; Gao, S. *Inorg. Chim. Acta* **1998**, *282*, 149−154. (e) Duarte, H. A.; Paniago, E. B.; Carvalho, S.; Dealmeida, W. B. *J. Inorg. Biochem.* **1998**, *72*, 71−77. (f) Roushdy, M. I.; Issa, Y. M.; Elzein, S. M.; Harb, F. M. S. E. *Asian J. Chem.* **1999**, *11*, 359−368. (g) Remko, M.; Mach, P.; Schleyer, P. V.; Exner, O. *J. Mol. Struct. (THEOCHEM*) **1993**, *98*, 139−150.
(15) (a) Muñoz-Caro, C.; Senent, M. L.; Ibeas, S.; Leal, J. M. *J. Org. Chem.*, **2000**, *65*, 405−410. (b) Ibeas, S.; García, B.; Leal, J. M.; Senent, M. L.; Niño, A.; Muñoz-Caro, C. *Chem.-Eur. J*. **2000**, *6* (14), 2644−2652.
(16) (a) Exner, O.; Hradil, M.; Mollin, J. *Collect. Czech. Chem. Commun.* **1993**, *58*, 1109−1121. (b) Bauer, L.; Exner, O. *Angew. Chem., Int. Ed. Engl*. **1974**, *13*, 376−384.
(17) (a) Ventura, O. N.; Rama, J. B.; Turi, L.; Dannenberg. J. J. *J. Am. Chem. Soc*. **1993**, *115*, 5754−576. (b) Ventura, O. N.; Rama, J. B.; Turi, L.; Dannenberg, J. J. *J. Phys. Chem*. **1995**, *99*, 131−136. (c) Tao, Y. Q.; Duan, W. G. *Int. J. Quant. Chem.* **1992**, *44*, 319−325. (d) Stinchomb, D. M.; Pranata, J. *J. Mol. Struct. (THEOCHEM*) **1996**, *370*, 25−32. (e) Yamin, L. J.; Ponce, C. A.; Estrada, M. R.; Tomas Vert, F. *J. Mol. Struct. (THEOCHEM)* **1996**, *360*, 109−117.
(18) García, B.; González, S.; Hoyuelos, F. J.; Ibeas, S.; Leal, J. M.; Senent, M. L.; Biver, T.; Secco, F.; Venturini, M. *Inorg. Chem.* **2007**, *46*, 3680−3687.

SCHEME 1. Most Stable Neutral and Anionic Structures of A-SHA Amide

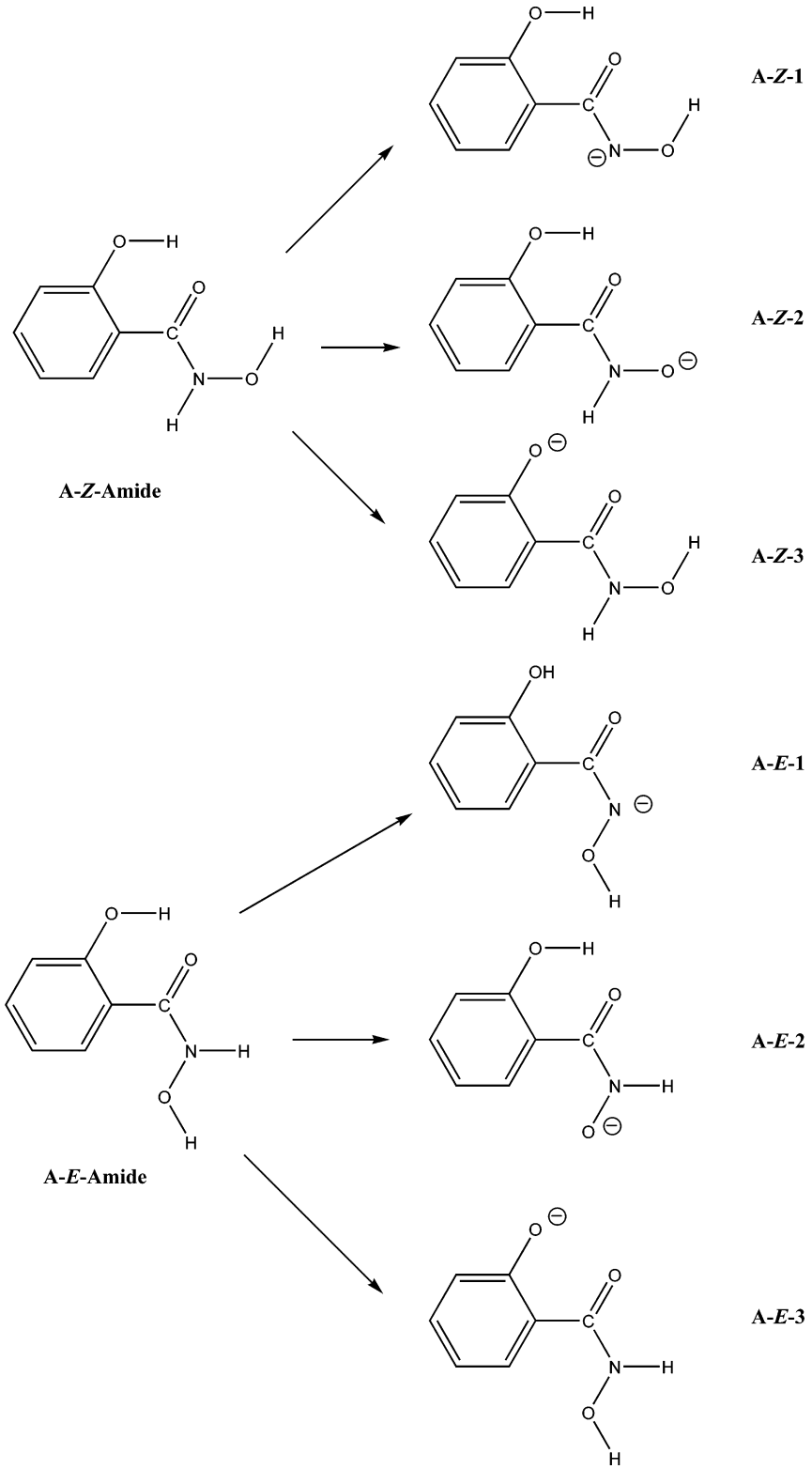

The A-*Z*-amide structure appears to be most stable in the gas phase; its most stable conformer, the B-*Z*-amide, lies 5.4 kcal/mol above the corresponding A-form. The A-*Z*-amide conformer becomes stabilized through formation of a strong intramolecular $O_PH\cdots O_C$ H-bond; actually, the most stable A-*E*-amide conformer lies 4.5 kcal/mol above the A-*Z*-amide form, in good agreement with the value reported by Kaczor et al.[19]

For the *Z*-amide, the most likely dissociation process is N-deprotonation, which requires 335.7 kcal/mol (A-SHA) and 329.6 kcal/mol (B-SHA), respectively. For the A-*E*-amide form, the most predictable dissociation process corresponds

(19) (a) Kaczor, A.; Proniewicz, L. M. *J. Mol. Struct.(THEOCHEM)* **2003**, *640*, 133−141. (b) Kazcor, A.; Szczepansky, J.; Vala, M.; Proniewicz, L. M. *Phys. Chem. Chem. Phys.* **2005**, *7*, 1960−1965.

TABLE 2. Comparison of p*K* Values of the Different Species at 25 °C

compound	pK_1	pK_2
p-hydroxybenzoic acid[a]	4.57	9.46
BHA[b]	8.78	
SHA[c]	7.56	9.85
PHBHA[c]	8.4	9.4

[a] Reference 26. [b] Reference 4. [c] This work.

to formation of anion A-*E*-2, which requires 340.5 kcal/mol. Table S2 shows the most likely dissociation processes of A-SHA and B-SHA calculated with the B3LYP/AUG-cc-pVDZ method.

Acid Dissociation Equilibria. UV Spectrophotometry. Evaluation of the p*K* values of SHA and PHBHA corresponding to the proton dissociation reactions 1 and 2

$$H_2A \overset{pK_1}{\rightleftharpoons} HA^- + H^+ \quad (1)$$

$$HA^- \overset{pK_2}{\rightleftharpoons} A^{2-} + H^+ \quad (2)$$

were carried out by UV−vis spectrophotometry.

SHA. Figure S1 shows the spectral changes recorded during the titration of SHA with NaOH. The data treatment used for equilibria evaluation has been described earlier.[5] The p*K* values at different temperatures (Table S3) are in good agreement with previously obtained data.[20−23] The temperature dependence of the pK_1 and pK_2 values yielded $\Delta H_1^0 = 4.4 \pm 0.4$ kcal mol^{-1} and $\Delta S_1^0 = -19.7 \pm 0.9$ cal mol^{-1} K^{-1} for reaction 1, and $\Delta H_2^0 = 3.6 \pm 0.1$ kcal mol^{-1} and $\Delta S_2^0 = -32.7 \pm 0.5$ cal mol^{-1} K^{-1} for reaction 2. The ΔS_2^0 value, more negative than the ΔS_1^0 value, accounts for the larger solvation of the dianion formed according to reaction 2. Both dissociation reactions are weakly endothermic.

PHBHA. The spectral changes recorded during the titration of PHBHA are shown in Figure S2; the absorbance vs pH plot at 258 nm (Figure 1), displaying a minimum at pH = 8.8, reveals overlapping equilibria. For pH > 7 the plot shows two unequal pH readings for the same absorbance value. This feature enables application of Ang's method.[24] This method is capable of analyzing and drawing a distinction between two ionization equilibria whose p*K* values lie very close to each other; the absorbance−pH data pairs can then be analyzed using eq 3,[25]

$$A = \frac{A_1(10^{-pH})^{m_1+m_2}(10^{-pK_1})^{-m_1}(10^{-pK_2})^{-m_2} + A_2(10^{-pH})^{m_2}(10^{-pK_2})^{-m_2} + A_3}{1 + (10^{-pH})^{m_2}(10^{-pK_2})^{-m_2} + (10^{-pH})^{m_1} + m_2(10^{-pK_1})^{-m_1}(10^{-pK_2})^{-m_2}} \quad (3)$$

where A_1 stands for the absorbance at the lowest pH value, A_3 for the absorbance at the highest pH value, and A_2 for the absorbance at intermediate acidity levels, all measured at the same wavelength. The m_i parameters were interpreted in terms of activity coefficients of the species involved in reactions 1 and 2. A nonlinear least-squares fitting of eq 3 to the data pairs yields the optimized values for A_1, A_2, A_3, m_1, m_2, pK_1 and pK_2; the continuous line measures the goodness of the fit. Table 2 lists the averaged pK_1 and pK_2 values that arose from replication of the fitting procedure at seven different wavelengths; also are included the p*K* values of those parent acids which may be useful to reliably give away the deprotonation sites.

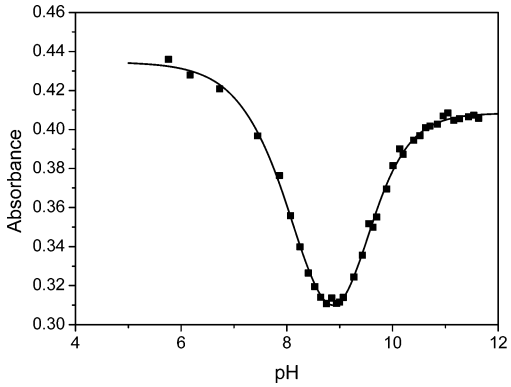

FIGURE 1. Dissociation process of PHBHA at $\lambda = 258$ nm. $T = 25$ °C, $I = 0.2$ M, and $C_{PHBHA} = 4.3 \times 10^{-5}$ M.

The closeness of the pK_2 values of SHA and PHBHA to the pK_2 value of *p*-hydroxybenzoic acid[26] suggests deprotonation at the $-O_PH$ site of the investigated acids. The pK_2 value of SHA is 0.5 units higher than that of PHBHA owing to the $O_P-H\cdots O_C$ hydrogen bond present only in this acid.

The pK_1 values deduced for SHA and PHBHA, rather close to that of benzohydroxamic acid (BHA), suggest that the hydroxamate group is the deprotonation site for both acids (Table 2). However, the pK_1 value of SHA was definitely lower than that of PHBHA. This feature could be interpreted if one takes for granted that the $O_P-H\cdots O_C$ hydrogen bond, present only in SHA, brings about a strength reduction of the adjacent $O_C\cdots H-O_H$ hydrogen bond, thus making deprotonation of the O_HH group easier. This interpretation requires that, in aqueous solution, both acids display the A-*Z* conformation. The difference in pK_1 values of SHA and PHBHA is almost twice the pK_2 difference. These results could not be interpreted only in terms of the different strength of the $O_C\cdots H-O_H$ hydrogen bond present in both acids; actually, due to the partial double bond character of the C−N bond, an electron-withdrawing effect from N to O_C becomes feasible; hence, N-deprotonation also becomes feasible. In the case of SHA the negative density of charge on O_C turns out to be reduced by the additional $O_P-H\cdots O_C$ hydrogen bond. As a consequence, an electron shift from N to O_C is favored, thus leading to a lower pK_1 value. To this aim, it is interesting to notice that simultaneous N and O_H deprotonation of SHA should occur in metallacrown formation.[27] Also, it should be noted that N-deprotonation concurs with the gas-phase computations performed on SHA.

^{1}H NMR Solution Study. PHBHA. The ^{1}H NMR spectrum of PHBHA in acetone (Figure 2a) displays several signals, in particular: (i) signal (1), which consists of three peaks, two very close together with same intensity; (ii) two small singlets,

(20) Agrawal, Y. K.; Tandon, S. G. *J. Electroanal. Chem.* **1973**, *43*, 158−160.
(21) Springer, V.; Hornackova, M.; Karlica, R.; Kopecka, B. *Collect. Czech. Chem. Commun.* **1987**, *52*, 602−608.
(22) Ciavatta, L.; De Tommaso, G.; Juliano, M. *Ann. Chim. (Rome)* **2004**, *94*, 295−302.
(23) Khalil, M. M.; Fazary, A. E. *Monatsh. Chem.* **2004**, *135*, 1455−1474.
(24) Ang, K. P. *J. Phys. Chem.* **1958**, *62*, 1109−1112.
(25) García, B.; Domingo, P. L; Leal, J. M. *Collect. Czech. Chem. Commun.* **1987**, *52*, 1087−1096.
(26) Sinistri, C.; Franzosini, P.; Riccardi, R. *Gazz. Chim. Ital.* **1959**, *89*, 1402−1414.
(27) Bodwin, J. J.; Cutland, A. D.; Malkani, R. G.; Pecoraro, V. L. *Coord. Chem. Rev.* **2001**, *216−217*, 489−512.

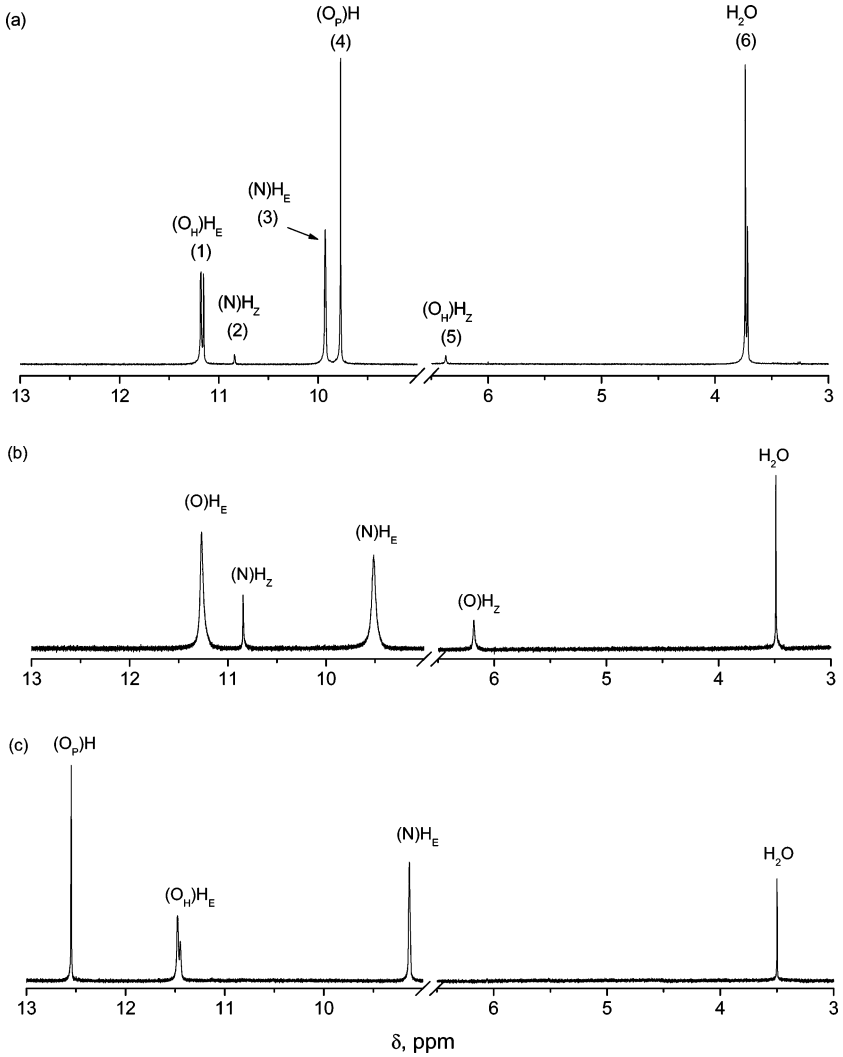

FIGURE 2. ^{1}H NMR spectra (400 MHz) recorded at −60 °C in acetone-d_6 for (a) C_{PHBHA} = 0.035 M, (b) C_{BHA} = 0.032 M, and (c) C_{SHA} = 0.02 M. For the sake of clarity, the signals of the aromatic H atoms are not shown.

(2) and (5), perceivable only below −10 °C; (iii) signal (3), whose location is strongly temperature- and concentration dependent; (iv) signal (4), which is only scarcely sensitive to the above variables, and (v) signal (6) that consists of two peaks, which are strongly temperature dependent and coalesce at 10 °C. The acetone signal, displayed at 2 ppm, is not reported in Figure 2. Two doublets centered at 6.81 and 7.75 ppm, whose locations are temperature- and concentration-independent, are also exhibited. They correspond to the aromatic hydrogen atoms and are not shown in Figure 2.

Considering the *Z/E* isomer effect, comparison of the spectra of PHBHA (Figure 2a) with those of benzohydroxamic acid (BHA)[5] (Figure 2b) makes clear that five of the observed signals in Figure 2a correspond to the signals shown in Figure 2b as follows: (1) corresponds to (O)H$_E$, (2) to (N)H$_Z$, (3) to (N)H$_E$, (5) to (O)H$_Z$, and (6) to H$_2$O. Hence, signals (1), (2), (3), and (5) will be denoted as (O$_H$)H$_E$, (N)H$_Z$, (N)H$_E$, and (O$_H$)H$_Z$, respectively. Signal (6), which consists of two close together singlets in PHBHA and only a singlet in BHA, corresponds to the trace water present in solution and will be analyzed below in connection with the NOESY experiments. The signal (4) displayed by PHBHA corresponds to the O$_P$H proton; this singlet, however, could not provide information on the PHBHA $Z \leftrightarrows E$ transition because the signals of both isomers overlap each other. Integration of the signals shown in Figure 2a yields the 4:96 *Z:E* population ratio; this ratio rises to 25:75 in BHA (Figure 2b) and falls down to 0:100 in SHA (Figure 2c).

Table S4 shows the PHBHA concentration effect on the 1−5 signals; these move downfield as the substrate concentration is raised, suggesting occurrence of PHBHA aggregation processes. Table S5 shows the temperature effect on the (O$_H$)H$_E$, (N)H$_Z$, (N)H$_E$, (O$_P$)H, and (O$_H$)H$_Z$ resonance in the −90−30 °C temperature range. Figure 3a shows the temperature effect on the (O$_H$)H$_E$, (N)H$_E$, and (O$_P$)H resonance in the −90−30 °C temperature range. The upfield shift observed when the temperature was raised can be put down to a reduction of the hydrogen bond strength present in the substrate structure. The most pronounced variation of the (N)H$_E$ proton signal suggests formation of *E*−*E* aggregates such as that shown in Figure 4a, similar to the dimer structures put forward for amides;[28] it should be noted that dimer formation has been suggested for other hydroxamic acids.[4,5,7,10,19] The somewhat more modest variation

(28) (a) Silverstein, R. M.; Webster, F. X. *Spectrometric Identification of Organic Compounds*, 6th ed.; Wiley & Sons: New York, 1998. (b) Scheiner, S. *Hydrogen Bonding: A Theoretical Perspective*; Oxford University Press: Oxford, 1997; p 125.

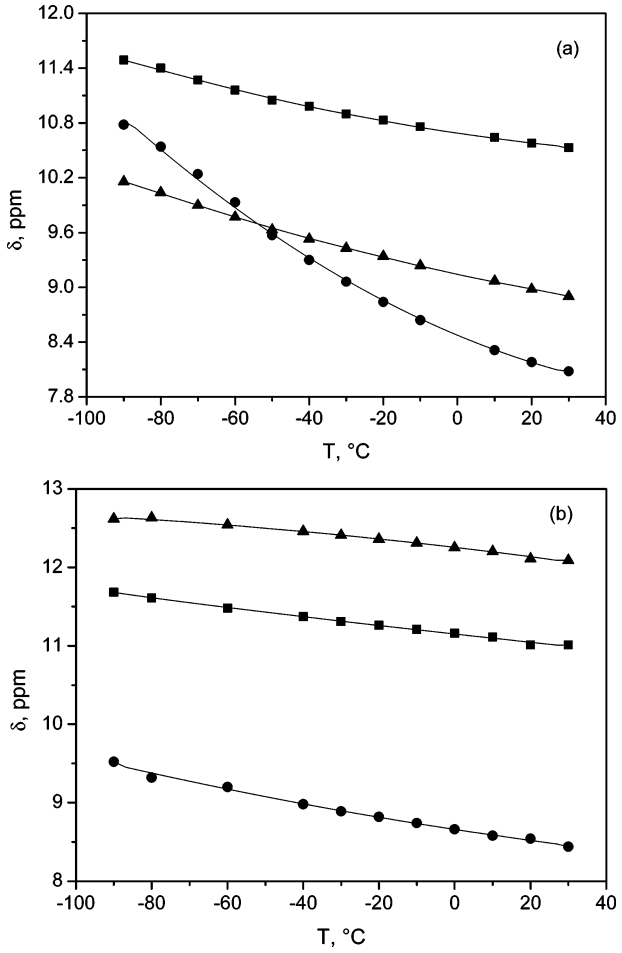

FIGURE 3. Temperature effect on the chemical shifts of the $(O_H)H_E$ (■), $(O_P)H$ (▲), and $(N)H_E$ (●) hydrogen atoms. (a) PHBHA (C_{PHBHA}= 0.035 M) and (b) SHA (C_{SHA}= 0.051 M).

of the other signals in Figure 3a, will be discussed below. The structure depicted in Figure 4a requires that, even if the monomers are in the *Z* conformation (as suggested by the theoretical calculations), those should adopt the *E* conformation for the dimerization process to occur. This idea is also consistent with the results of a previous NMR study of BHA,[5] where the *E* isomer was found to be the majority species in acetone at low temperature.

The gas-phase relative stabilities of the *E*−*E* and *Z*−*E* PHBHA dimers, calculated with B3LYP/cc-pVDZ, show that the *E*−*E* dimer (μ = 0.0441 D) is more stable by 9.0 kcal mol^{-1} than the *Z*-*E* dimer (μ = 4.8056 Debye). Calculations for the *Z*−*Z* structure did not attain convergence. In conclusion, both the NMR spectra and the theoretical calculations point to formation of *E*−*E* dimers.

Figure 5 shows the concentration dependence of the signal (3) corresponding to the $(N)H_E$ proton at −60 °C (Figure 2a). The signal moves downfield as the PHBHA concentration is boosted, concurrent with the onset of intermolecular hydrogen bonds corresponding to the presence of aggregates in equilibrium with monomers; the signal tends to level off at the highest substrate content, suggesting that under these circumstances the aggregated forms tend to prevail. On the other hand, measurements at 20 °C (not shown) reveal that the $(N)H_E$ chemical shift is independent of the PHBHA concentration, suggesting that at high temperature only monomers are present.

Figure 6a shows more in detail how signal (1), corresponding to the$(O_H)H_E$ proton (Figure 2a), changes when the PHBHA total concentration is varied. The observed inversion of the peak integral ratio as the substrate concentration is raised, clearly indicates occurrence of aggregation, the two signals with the same intensity corresponding to the aggregate. If the aggregation process is described by

$$n\mathrm{A} \rightleftarrows \mathrm{A}_n \qquad (4)$$

then the *n* value can readily be obtained through a log−log plot according to

$$\log R = \log K_n + (1 - n) \times \log\left(\frac{1 + n\mathrm{R}}{C_\mathrm{A}}\right) \qquad (5)$$

where R = [aggregate]/[monomer], C_A is the total substrate concentration and K_n is the equilibrium constant of reaction 4. Derivation of eq 5 is shown in detail in SI. The *n* and K_n parameters are obtained by an iteration procedure; once the convergence is reached, the slope of such a plot yields the value n = 3.3, and the intercept yields $K_n = 4.5 \times 10^5$ M^{1-n} (Figure 7). These results indicate that the PHBHA aggregates are more complex than simple dimers. The value of *n* higher than three suggests that probably some tetramer structures could also be present.

It is interesting to notice that the $(N)H_E$ signal is single, whereas the $(O_H)H_E$ signal is split into two peaks. This fact indicates that the chemical process associated with the $(N)H_E$ signal is fast even at low temperatures, consistent with formation of hydrogen bonds as in the dimer structures of Figure 4. The

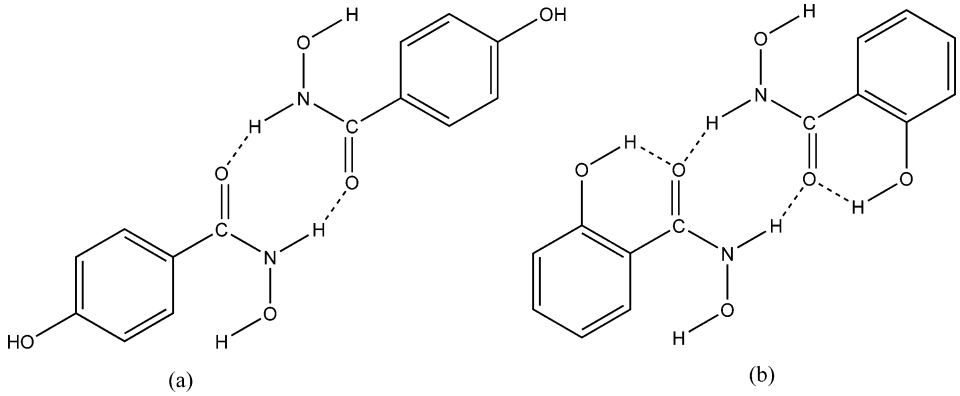

FIGURE 4. Dimer structures: (a) *E*-PHBHA, and (b) A-*E*-SHA.

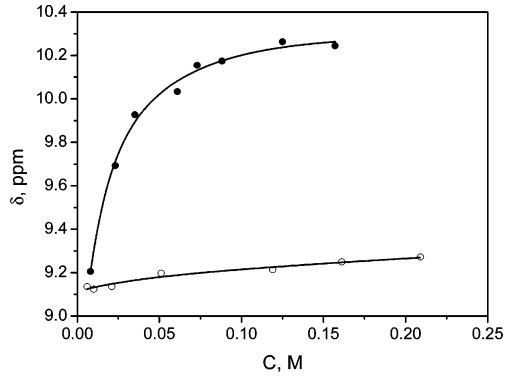

FIGURE 5. Concentration effect on the chemical shift of the peak associated with the (N)H_E proton recorded in acetone at $T = -60$ °C: (●) PHBHA, and (○) SHA.

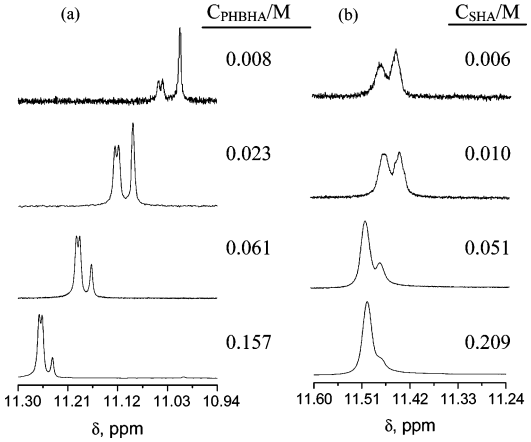

FIGURE 6. Portion of the 400 MHz ^{1}H NMR spectra showing the concentration effect on the (O_H)H_E proton signals recorded at −60 °C in acetone-d_6 for (a) PHBHA and (b) SHA.

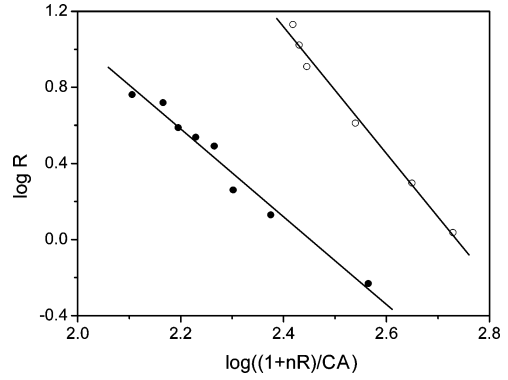

FIGURE 7. Analysis of the concentration effect on the peaks of the (O_H)H_E protons (eq 5) recorded at $T = -60$ °C in acetone: (●) PHBHA, (○) SHA.

rates for the monomer ⇆ dimer interconversion are expected to be diffusion-controlled. For instance, ultrasonic relaxation measurements on aqueous *N*-ethylacetamide show that the monomer−dimer interconversion is very fast ($\tau = 6-8 \times 10^{-9}$ s at −10 °C).[29] By contrast, the (O_H)H_E signal splitting is associated to a slower process. According to the structures of Figure 4 this proton is not directly involved in dimer formation. However, it can be involved in tetramer structures as will be shown later; in such a case, the formation of π-stacked aggregates can well give separate peaks, i.e., the momomer ⇆

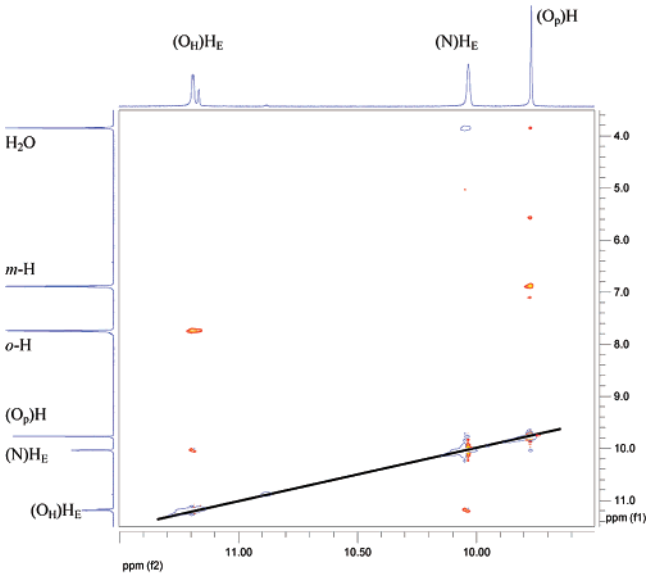

FIGURE 8. ^{1}H−^{1}H NOESY spectrum of PHBHA in acetone-d_6. $T = -60$ °C, C_{PHBHA}= 0.061 M. The 400 MHz ^{1}HNMR spectrum is shown at the top and left-hand edges, with assignments.

π-aggregate exchange rate is slow on the NMR time scale. For instance, the π-aggregation process of the cyanine CCyan2, studied in aqueous solution at 25 °C by the T-jump technique, was found to occur on a much longer time scale (0.2−1 millisecond for substrate concentrations of the orders of 1×10^{-4} M).[30]

Figure S3 shows the ^{1}H−^{1}H NOESY spectra of PHBHA recorded in acetone at −60 °C. Figure 8 shows the expansion of the most relevant peaks. Only a cross-peak due to chemical exchange (with the same phase as the diagonal, continuous line), but five cross-peaks from NOE interactions (with opposite phase than the diagonal) could be observed. A NOE interaction between the (O_H)H_E proton and the aromatic hydrogen atoms in the ortho position with respect to the hydroxamate group was observed at (7.75, 11.19). The cross-peak at (9.77, 6.89) corresponds to the NOE interaction between the aromatic meta hydrogen atoms and the (O_P)H hydrogen. The signal at (11.18, 10.03) indicates the NOE interaction between (N)H_E and (O_H)-H_E; all these cross-peaks verify the signal assignment shown in Figure 2a. As expected, the NOE cross-peak at (6.89, 7.75) corresponds to the interaction between the *o*-H and *m*-H aromatic hydrogen atoms (only shown in Figure S3). Concerning the aggregate structures, it is interesting to note that a small NOE corresponding to the interaction between (O_P)H and one of the signals assigned to water appeared at (9.77, 3.84).

In the ^{1}H NMR spectrum, the two water peaks (signal 6) behave differently. The peak area at $\delta = 3.85$ ppm rises upon addition of small water amounts to the acetone-d_6 solution, whereas the peak area at $\delta = 3.84$ ppm remains constant. It can then be concluded that the signal at $\delta = 3.85$ ppm corresponds to the free water present in solution. On the other hand, the peak area at $\delta = 3.84$ ppm is proportional to the PHBHA content, the 2:1 PHBHA:H_2O ratio indicating that the signal at $\delta = 3.84$ ppm corresponds to the stoichiometric water joined to solute.

(29) Miecznik, P. *J. Chem. Phys.* **1999**, *10*, 2539−2543.
(30) Biver, T.; De Biasi, A.; Secco, F.; Venturini, M.; Yarmoluk, S. *Biophys. J.* **2005**, *89*, 374−383.

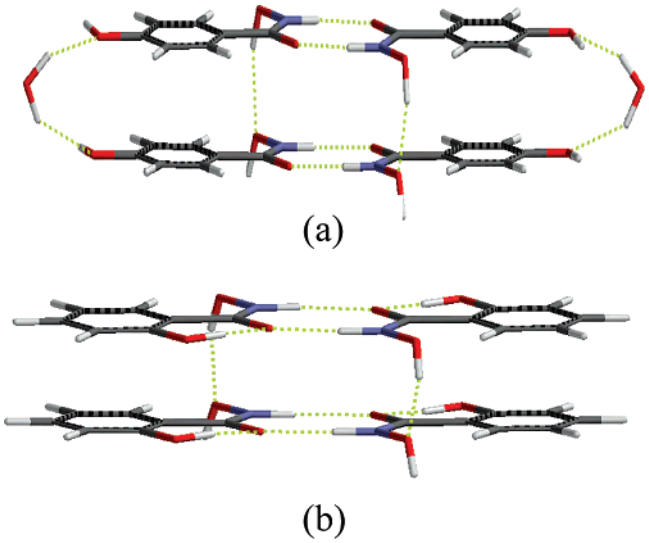

FIGURE 9. Suggested tetramer structures for (a) PHBHA, and (b) A-SHA.

The outcomes of the NMR experiments concur in supporting a sandwich-like structure of the PHBHA aggregate, where two dimers of the type shown in Figure 4a gather together to form a tetramer stabilized by two water molecules (Figure 9a); the value $n = 3.3$ deduced by application of eq 5 bears out this interpretation. Likewise, hydrogen bonds such as $(O_H)H_E \cdots O_H$ and $\pi-\pi$ interactions are also important for the tetramer stabilization. This issue will be discussed below concurrently with the analysis of the SHA NMR experiments. The analysis of the NMR spectra according to eq 5 and the 1D and 2D ^{1}H NMR experiments enables one to conceive the aggregation process in a more detailed way according to reaction 6

$$4A \rightleftarrows 2A_2 \rightleftarrows A_4 \qquad (6)$$

where the steady-state concentration of species A_2 is in the minority. On this basis, the two signals with same intensity shown in Figure 6a correspond to the tetramer, and the signal at higher field corresponds to the monomer. The even intensity of the two signals could be interpreted in light of the tetramer structure put forward in Figure 9a. Two of the four $(O_H)H_E$ hydrogen atoms present in the tetramer are involved in $(O_H)H_E \cdots (O_H)H_E$ interdimer bonds, and the other two are free. The small signal separation and the broad shape both suggest an interchange between the hydrogen-bonded and the free $(O_H)H_E$ groups. Finally, it should be noticed that $\pi-\pi$ vertical interactions could add further stability to the tetramer structure. In principle, vertical interactions such as $(O_P)H-\pi$ and/or $(O_H)H-\pi$ are also feasible in the proposed tetramer structure.[31] Such interactions should alter the chemical shift of the aromatic protons; however, in view of the ^{1}H NMR experiments that demonstrated this is untrue, this sort of interaction was not taken into consideration.

SHA. Compared to the ^{1}H NMR behaviors of PHBHA and BHA, that of SHA (Figure 2c) is simpler. In addition to the water peak, only three signals could be observed which, by comparison with the spectra of PHBHA and BHA, will be assigned to the *E* isomer, which appears to be in the majority. The signals of the aromatic hydrogens do not exhibit any variation of chemical shift with temperature and substrate concentration and therefore are not included here. The location of the two rather close signals at about 11.4 ppm, corresponding to the $(O_H)H_E$ proton, is almost concentration independent; however, its relative intensity strongly changes with the rise in SHA concentration, as shown in detail in Figure 6b. This behavior resembles that of PHBHA and suggests that SHA also undergoes self-aggregation. The parameters deduced for SHA by application of eq 5, $n = 4.0$ and $K_n = 2.2 \times 10^8$ M^{1-n} (Figure 7), reveal that in this system the tetramer formation is more extended compared to that in PHBHA. However, formation of aggregates with higher *n* for higher substrate concentrations could not be ruled out. Absence of splitting of the low-field component of the $(O_H)H_E$ pair of signals observed for SHA could be rationalized by assuming that the rate of proton exchange is higher in the SHA tetramer compared to that in PHBHA. By analogy with the corresponding signals observed for PHBHA and BHA, the signal ranging between 8.4 and 9.5 ppm (Figures 2c and 3b) has been assigned to the $(N)H_E$ proton, since its line width at 20 °C and its location in the spectrum concur with the observed behavior of the amide NH proton.[28]

The sharp peak at 12.6 ppm corresponds to the $(O_P)H_E$ proton. The chemical shift ($\delta > 12$ ppm) observed for this proton, much larger than that of PHBHA ($\delta < 10$ ppm), should be put down to the strong $O_P-H\cdots O_C$ hydrogen bond present in SHA. The signal at 3.45 ppm (Figure 2c) corresponds to trace water; contrary to the two signals of water observed for PHBHA (Figure 2a), the water signal for SHA is a single signal whose intensity is independent of the SHA concentration and corresponds to the free water. This observation suggests that water molecules, which stabilize the tetramer PHBHA structure (Figure 9a), are absent in the case of tetramer SHA (Figure 9b). The enhanced stability of the SHA aggregate, borne out by the larger K_n value, could be explained by the extended planarity of the *E*−*E* dimer moieties (Figure 4b) forming the tetramer, which would result in an increase of the $\pi-\pi$ interactions. In addition, further stabilization of the SHA tetramer can arise from the enhanced strength of the vertical hydrogen bonds, revealed by the downfield δ shift of the $(O_H)H_E$ proton of SHA compared to that of PHBHA (Table 4S and Figure 6). Figure 5 shows that the concentration effect on the chemical shift of the SHA $(N)H_E$ proton is more restricted compared to that of PHBHA; this behavior finds a convincing explanation in the enhanced stability of the SHA tetramer. Actually, since the equilibrium represented by reaction 4 shifted toward the SHA tetramer ($K_n = 2.2 \times 10^8$ M^{-3}), the concentration dependence of δ should level off at relatively low substrate concentrations. Figure 5 also shows that, at relatively high substrate concentration, the $(N)H_E$ chemical shift drops by about 1 ppm on going from PHBHA to SHA. Such an effect can be put down to the strength reduction of the $(N)H_E \cdots O_C$ intermolecular hydrogen bond in SHA, brought about by the presence of a second strong intramolecular $(O_P)H\cdots O_C$ hydrogen bond (Figure 4b). The temperature dependence of the chemical shifts shown in Figure 3 bears out the above observations. The decrease in δ for $(N)H_E$ upon rising temperature is much more pronounced for PHBHA compared to that for SHA, concurrent with the less stable structure of the PHBHA aggregates.

(31) Desiraju, G. R.; Steiner, T. *The Weak Hydrogen Bond: Applications to Structural Chemistry and Biology*; International Union of Crystallography Monographs on Crystallography, 9; Oxford University Press: Oxford New York, 1999; (a) p 130. (b) pp 363−364.

Experimental and Computational Section

All chemicals were analytical grade. Hydroxamic acids, SHA and PHBHA, were recrystallized from water; to reduce to a maximum the water content, the crystals were dried for 48 h under vacuum in an inert nitrogen atmosphere. Acetone was purified as previously described.[4] Despite the many cautions taken, full exclusion of water from the solution was unattainable.

All the NMR experiments were performed using a 400 MHz instrument (operating at 399.94 MHz for ^{1}H). Two-dimensional NOESY NMR spectra were carried out for PHBHA in acetone-d_6 at −60 °C. The chemical shifts were referenced to the residual resonance of the deuterated solvent. The sample temperature was calibrated with a standard methanol sample.

The spectrophotometric measurements were performed with a Hewlett-Packard 8453 spectrophotometer with a Peltier accessory to control temperature. Experiments were performed at 15, 25, 35, 45, and 55 °C for SHA and at 25 °C for PHBHA. In view that some benzohydroxamic acids may undergo hydrolysis in basic medium,[32] the conditions for such an effect to be negligible were carefully controlled. The reversibility of the acid−base process was routinely checked. To properly remove the CO_2 dissolved in water, the spectra were recorded in an inert atmosphere. The pH readings were taken by a pH meter, with a glass electrode combined with a 3 M KCl calomel electrode and temperature probe, equilibrium time 120 s and a 20 mV/min signal drift. The glass electrode was calibrated with eight buffer solutions covering the 1.26−12.46 pH range, which enables a fair coverage of the acidity range of the experiments with a single calibration curve.

To reduce to a minimum the computational effort, all calculations were performed with the Möller−Plesset perturbation (MP2/RHF/cc-pVDZ) and density functional theory (B3LYP). Both theoretical approximations, MP2 and B3LYP, bear identical accuracy for the determination of equilibrium geometries. All the calculations were carried out with the package Gaussian 98.[33]

The calculations have been initialized at the RHF/cc-pVDZ level, which is powerful enough for the search for the minimum energy structures optimizing the geometry from distinct starting points. More accurate B3LYP/AUG-cc-pVDZ calculations, with full geometry optimization, have been performed from the RHF structures for determining the relative energies and the enthalpies of the likeliest deprotonation processes.

Acknowledgment. The financial support by Ministerio de Educación y Ciencia, Project CTQ2006-14734/BQU, Junta de Castilla y León, Project BU 001A-06, and DGESIC (Grant PM98-0073), Spain, are gratefully acknowledged.

Supporting Information Available: ^{1}H NMR data, UV spectra and thermodynamic parameters for acid dissociation of SHA and PHBHA, computational data of SHA, derivation of eq 5. This material is available free of charge via the Internet at http://pubs.acs.org.

JO0709798

(32) Ghosh, K. K.; Rajput, S. K.; Krishnani, K. K. *J. Phys. Org. Chem.* **1992**, *5*, 39−43.

(33) Frisch, M. J.; Trucks, G. W.; Schlegel, H. B.; Scuseria, G. E.; Robb, M. A.; Cheeseman, J. R.; Zakrzewski, V. G.; Montgomery, J. A., Jr.; Stratmann, R. E.; Burant, J. C.; Dapprich, S.; Millam, J. M.; Daniels, A. D.; Kudin, K. N.; Strain, M. C.; Farkas, O.; Tomasi, J.; Barone, V.; Cossi, M.; Cammi, R.; Mennucci, B.; Pomelli, C.; Adamo, C.; Clifford, S.; Ochterski, J.; Petersson, G. A.; Ayala, P. Y.; Cui, Q.; Morokuma, K.; Salvador, P.; Dannenberg, J. J.; Malick, D. K.; Rabuck A. D.; Raghavachari, K.; Foresman, J. B.; Cioslowski, J.; Ortiz, J. V.; Baboul, A. G.; Stefanov, B. B.; Liu, G.; Liashenko, A.; Piskorz, P.; Komaromi, I.; Gomperts, R.; Martin, R. L.; Fox, D. J.; Keith, T.; Al-Laham, M. A.; Peng, C. Y.; Nanayakkara, A.; Challacombe, M.; Gill, P. M. W.; Johnson, B.; Chen, W.; Wong, M. W.; Andres, J. L.; Gonzalez, C.; Head-Gordon, M.; Replogle, E. S.; Pople, J. A.; *Gaussian* 98, revision A1; Gaussian, Inc.: Pittsburgh PA, 2001.